IOPscience iopscience.iop.org

Home Search Collections Journals About Contact us My IOPscience

Optical signatures of intrinsic electron localization in amorphous SiO_2

This content has been downloaded from IOPscience. Please scroll down to see the full text.

2015 J. Phys.: Condens. Matter 27 265501

(http://iopscience.iop.org/0953-8984/27/26/265501)

View the table of contents for this issue, or go to the journal homepage for more

Download details:

IP Address: 128.41.35.62

This content was downloaded on 19/08/2016 at 17:35

Please note that terms and conditions apply.

You may also be interested in:

Structure and properties of defects in amorphous silica

Peter V Sushko, Sanghamitra Mukhopadhyay, Andrey S Mysovsky et al.

Modelling of electron and hole trapping in oxides

A L Shluger, K P McKenna, P V Sushko et al.

Oxygen deficient centers in silica: optical properties within many-body perturbation theory

N Richard, L Martin-Samos, S Girard et al.

Trapping, self-trapping and the polaron family

A M Stoneham, J Gavartin, A L Shluger et al.

Photoionization processes in barium fluorohalidecrystals

E Radzhabov and T Kurobori

Simulation of the oxygen vacancy

M Busso, S Casassa, C Pisani et al.

Small polarons in real crystals: concepts and problems

A L Shluger and A M Stoneham

OPEN ACCESS
IOP Publishing

Journal of Physics: Condensed Matter

J. Phys.: Condens. Matter **27** (2015) 265501 (6pp)

doi:10.1088/0953-8984/27/26/265501

Optical signatures of intrinsic electron localization in amorphous SiO_2

A-M El-Sayed[1], **K Tanimura**[2] **and A L Shluger**[1]

[1] Department of Physics and Astronomy and London Centre for Nanotechnology, University College London, Gower Street, London, WC1E 6BT, UK
[2] The Institute of Scientific and Industrial Research (ISIR), Osaka University, Mihogaoka 8-1, Ibaraki, Osaka 567-0047, Japan

E-mail: al-moatasem.el-sayed.10@ucl.ac.uk

Received 5 March 2015, revised 16 April 2015
Accepted for publication 8 May 2015
Published 8 June 2015

Abstract

We measure and analyse the optical absorption spectra of three silica glass samples irradiated with 1 MeV electrons at 80 K, where self-trapped holes are stable, and use *ab initio* calculations to demonstrate that these spectra contain a signature of intrinsic electron traps created as counterparts to the holes. In particular, we argue that optical absorption bands peaking at 3.7, 4.7, and 6.4 eV belong to strongly localised electrons trapped at precursor sites in amorphous structure characterized by strained Si–O bonds and O–Si–O angles greater than 132°. These results are important for our understanding of the properties of silica glass and other silicates as well as the reliability of electronic and optical devices and for luminescence dating.

Keywords: electron traps, optical absorption, excited state

(Some figures may appear in colour only in the online journal)

1. Introduction

Electron and hole localization in disordered solids is fundamental for many applications. However, strong localization in complex 3D systems is material specific and difficult to elucidate, as has been demonstrated by recent studies of a wide range of materials, such as feldspar [1], semiconducting polymers [2], olivine phosphates [3], and porous amorphous water ice [4]. Electron and hole localization in disordered oxides is particularly important for many applications, such as reliability and radiation stability of microelectronic devices, formation processes in resistive memory devices, performance of optical fibres, and luminescence dating, to mention a few. Amorphous silica (a-SiO_2) is a classic disordered oxide which, although studied for decades, still puzzles researchers. It has been demonstrated, both experimentally [5, 6] and theoretically [7, 8], that holes can trap at intrinsic network sites in irradiated a-SiO_2 forming self-trapped holes (STH) which are stable below 180 K. However, there is no clear understanding of the whereabouts of their corresponding electrons, which are often assumed to be trapped by impurities (e.g. Ge, Al) or at other defect sites.

Unambiguously identifying all sites responsible for electron trapping in a-SiO_2 has proved particularly challenging because of a large number of possible charge redistribution channels and the presence of water and impurities in most samples. In fact, there are numerous unexplained examples of electron trapping resulting from electron injection into a-SiO_2 in Si/SiO_2 devices at room temperature, some of which are attributed to pre-existing defects [9–14]. On the other hand, recent calculations predict that an extra electron can localize in non-defective a-SiO_2 networks accompanied by a strong local distortion of a SiO_4 tetrahedron [15, 16]. Unusually, these very deep, strongly localized intrinsic electron states are formed in a material with a low (3.9) static dielectric constant. Moreover, similar electron localization is predicted to occur in crystalline quartz, albeit with much higher barriers than for glass. The disordered glass structure was shown to contain structural (so-called precursor) sites which favour electron localization. Despite these theoretical results, unambiguous

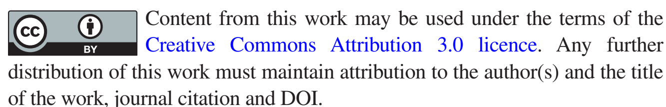
Content from this work may be used under the terms of the Creative Commons Attribution 3.0 licence. Any further distribution of this work must maintain attribution to the author(s) and the title of the work, journal citation and DOI.

 © 2015 IOP Publishing Ltd Printed in the UK

experimental evidence of intrinsic electron trapping in a-SiO_2 is still missing.

In this paper we measure and analyse the optical absorption spectra of three different silica glass samples irradiated at 80 K, where trapped electrons could co-exist with self-trapped holes, and use theoretical calculations to suggest that these spectra contain a signature of intrinsic electron traps.

2. Experimental observations

Three different, high-purity a-SiO_2 samples were used in this study to differentiate the results that are specific to only a given sample from those that are common to all samples. These include Suprasil W1 (SW1), Viosil-SCF (SCF), and Viosil-SZ (SZ); all fabricated by Shin-Etsu Quartz, LTD. SW1 has less than a few ppm of OH ions, but includes a considerable amount of dissolved O_2. SZ includes almost no chemical impurities—concentrations of both Cl and OH ions are less than 1 ppm—however, it includes 500 ppm of oxygen deficiency (so called ODC(I)) centres that exhibit a strong absorption peak at 7.6 eV and its fundamental absorption edge was measured at 8.0 eV. On the other hand, SCF has no Cl ions (less than 1 ppm), but includes about 1000 ppm of OH ions. All samples were cut and polished to a size of $8 \times 10 \times 1$ mm and irradiated with electron beams (1 MeV, 20 ns duration) generated from a Febetron (HP43710A) at 80 K. The optical absorption spectra were measured after the irradiation using a spectrophotometer (Shimazu UV-3100). A Xe-arc lamp was used as the light source for optical excitation of the irradiated specimens. Red light with a wavelength range from 600 to 780 nm, and UV light with a peak at 320 nm (3.87 eV) and a band pass of 10 nm was generated by combining appropriate optical filters.

The black curve in figure 1(a) shows the optical absorption spectrum induced by the electron irradiation at 80 K in the SZ sample. Several peaks are clearly distinguishable. The lowest-energy peak at 2.2 eV has been attributed to self-trapped holes with two-centre type configurations (STH2) [17]. The peaks at 5.1 and 5.7 eV are associated with B2 and E′ centres (3-coordinated Si dangling bond), respectively. We note that the origin of the absorption bands around 4.5–5.0 eV depends critically on the samples employed. In fact, in the SZ sample with a significant amount of ODC(I), the dominant contribution comes from the B2 centre (see figure 1(a)). In the SCF sample, which includes OH ions, non-bridging oxygen hole centres, which show an absorption peak at 4.8 eV, are the dominant contributor, while in SW1, which includes dissolved oxygen, the ozone centres contribute primarily at 4.8 eV. These are typical examples of specimen-dependent features of absorption bands. On the other hand, the peak with a maximum at 3.7 eV is an, as yet, unattributed band, which is commonly generated in a-SiO_2 samples irradiated and measured at low temperatures and thus is not related to specific pre-existing atomistic defects in a-SiO_2 network. The strong absorption peaking at >6.5 eV is usually attributed to ODC(II) or B2 centres [18]. We note that similar peaks with almost the same heights have been generated in SW1 and SCF samples, which contain almost no oxygen vacancies (see figure 2 in [17]).

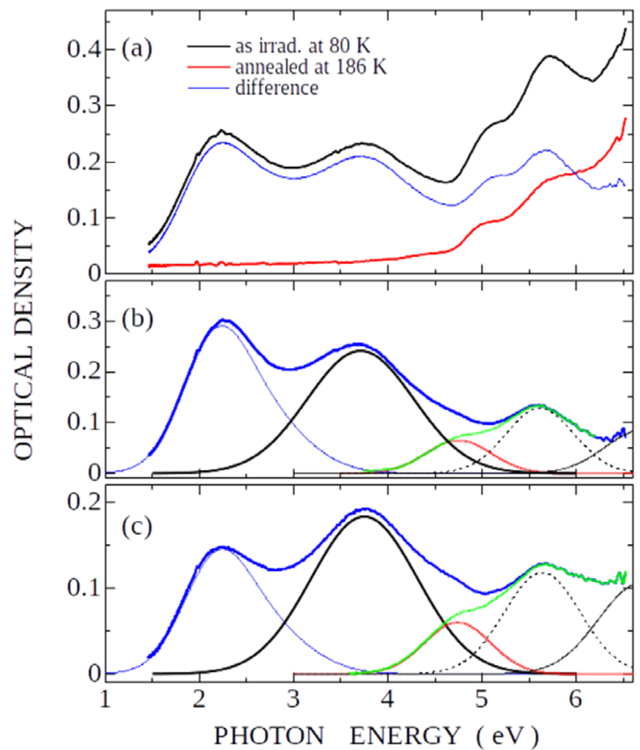

Figure 1. (a) Optical absorption spectra of electron-irradiated a-SiO_2(SZ). The black curve was recorded at 80 K after electron irradiation. The red curve was recorded at 80 K after anneal at 186 K. The blue curve is the difference between the black and red curves, revealing the absorption components due to centres annihilated during anneal. (b) and (c) show the difference spectra between the absorption bands of electron-irradiated a-SiO_2 and those after selective excitation: (b) by red light (600–780 nm) and (c) by UV light (320 ± 10 nm). The difference spectra are deconvoluted into the absorption bands due to STH2 (thin blue solid curve at 2.2 eV), a 3.7 eV band (thick solid curve), and the rest of the spectrum (solid green curve), which are decomposed further into a 4.7 eV band (thin red curve), the E′ centre band (broken curve centred at 5.8 eV) and the 6.6 eV band (thin solid curve).

To reveal the origin of the 3.7 eV band, we measured its growth kinetics as a function of electron dose. In figure 2, the growth characteristics of the E′ centres (5.7 eV), STH2 (2.2 eV), and the 3.7 eV absorption band are shown. The yield of E′ centres increases linearly with the dose, while those of the STH2 and the unattributed centre are strongly correlated and show a tendency to saturate at doses greater than $\approx 1.5 \times 10^5$ Gy, indicating that the STH2 and 3.7 eV peak grow concurrently. One of the reasons for saturation could be that the number of precursor sites for trapped holes is limited and smaller than the number of oxygen vacancies in SZ samples.

The thermal stability of the defects responsible for the optical absorption spectrum in figure 1(a) was studied by a pulse annealing method. The red line in figure 1(a) shows the absorption spectrum after warming the irradiated sample up to 186 K (at which STHs are mobile) for 5 min, followed by an absorption measurement at 80 K. One can see that the peaks at 2.2 and 3.7 eV are completely annealed out, which is also demonstrated by the blue curve showing the difference

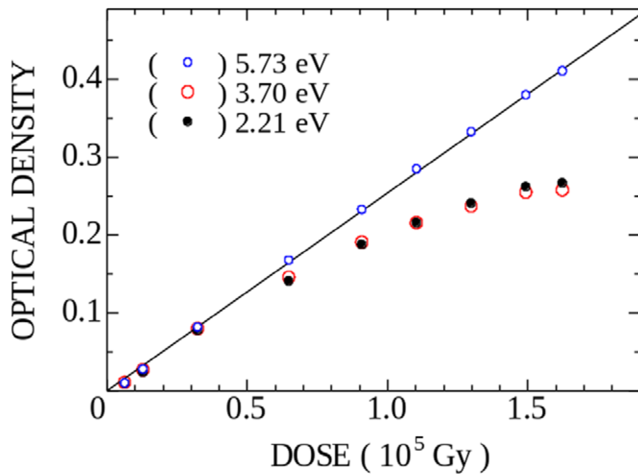

Figure 2. Growth kinetics of the optical absorption bands of electron irradiated a-SiO_2 measured at 80 K. The 2.21 eV and 3.70 eV peaks show a trend to saturate at a dose greater than 1.5×10^5 Gy.

between the initial low temperature electron irradiation and the post-anneal spectra. This data again supports the notion that the STH2 and 3.7 eV peaks are strongly correlated. We note that the absorption bands with energies above 4.5 eV, mostly due to B2 and E′ centres, are significantly reduced after annealing at 186 K. These are characteristic features of low-temperature irradiated glass samples, as B2 and E′ centres themselves are thermally stable even at 300 K.

Optical bleaching experiments at 80 K can shed more light on the origins of these absorption spectra by releasing trapped holes and electrons back into valence and conduction bands, respectively, as a result of selective excitation. Figure 1(b) exhibits a difference spectrum of the sample before and after bleaching by red light (600–780 nm), which selectively excites only STH2. This excitation results in a significant depletion of the 3.7 eV band, as well as other higher energy bands. Interestingly, the B_2 band is little affected by the excitation, although a substantial amount of the E′ band is bleached. Similarly, figure 1(c) shows the spectral components after selective excitation by UV light (320 ± 10 nm). The excitation in the 3.7 eV band also results in a high degree of bleaching of the 2.2 eV band and some of the higher energy bands including that of the E′ centre, although the B2 band is again little affected. Figures 1(b) and (c) also demonstrate that the decay of the 3.7 eV band is always associated with the decay of the spectral components around 4.7 eV and above 6 eV. This feature is characteristic to all samples studied in this work, regardless of the differences in composition of the a-SiO_2 network.

The ratio between the STH2 band and the 3.7 eV band changes differently in the two photo-bleaching events, demonstrating that they are indeed associated with different centres. The fact that their creation and annihilation are strongly correlated leads us to suggest that the centre giving rise to the 3.7 eV absorption band is likely to be an electron partner of STH2 created by the electron irradiation. It is known that electrons can trap on pre-existing oxygen vacancies [19], impurities, or at intrinsic network sites in a-SiO_2 [16]. The calculated position of the maximum of the optical absorption of negatively charged oxygen vacancies is at about 3.3 eV [19] and they can contribute to the 3.7 eV absorption in SZ samples which include a considerable amount of oxygen vacancies. Some oxygen excess silica samples exhibit a relatively weak absorption band at 3.8 eV. This band had initially been attributed to peroxy linkages, but was later shown to be due to interstitial Cl_2 molecules [20]. However, as noted above, the 3.7 eV band is induced in all of the SW1, SZ and SCF samples regardless of whether they include dissolved oxygen, OH ions or pre-existing oxygen vacancies. Therefore, we can exclude these defects from being the source of the 3.7 eV band in this study. The remaining candidate is an electron trapped by the amorphous SiO_2 network [16].

3. Theoretical calculations

To further investigate the atomistic origins of the 3.7 eV and other absorption bands in figure 1, we calculated the optical transitions of intrinsic electron trapping centres in a-SiO_2 using an embedded cluster method implemented in the GUESS code [21]. The effect of structural disorder in glass samples on inhomogeneous broadening of absorption spectra is included by using seven independent models of a-SiO_2. These were produced using the ReaxFF forcefield [22] and molecular dynamics simulations to melt samples of crystalline β-cristobalite at 5000 K and then quench them to 0 K. This procedure is explained in detail in a previous publication [16].

These models were then adapted for use in an embedded cluster model where each a-SiO_2 matrix was represented as a spherical nanocluster divided into two regions—I and II. Region I is located in the centre of the nanocluster and is further subdivided into three concentric regions of different physical descriptions. The centre of region I consists of a cluster of atoms which are treated using density functional theory (DFT) implemented in the Gaussian09 code. The Si and Ge atoms are described with a 6-31G* basis set and the O atoms with a 6-31G basis set. The outer section of region I is described by a core-shell variant of the classical BKS potential [23]. The central quantum region is interfaced with the outer classical ions by embedding pseudopotentials [23, 24]. The outer region II is composed of non-polarizable ions which are fixed in perfect lattice sites and interact with ions in region I by the classical BKS potential, which does not include shells [25]. All atoms in region I are allowed to relax during geometry optimizations to provide the atomic structure of the electron traps.

We used a hybrid BxLYP functional with $x = 32.5\%$ exchange, which provides a better band description than the B3LYP functional [26] and improves the linearity of the functional [27]. The optical absorption spectra of the electron traps were then calculated using the time-dependent DFT (TDDFT) method [28], as implemented in the Gaussian09 code.

3.1. Optical absorption of the Ge electron centre

To test whether this method provides an accurate description of the optical absorption spectrum of localized electron centres in SiO_2, we calculated the optical absorption spectrum of

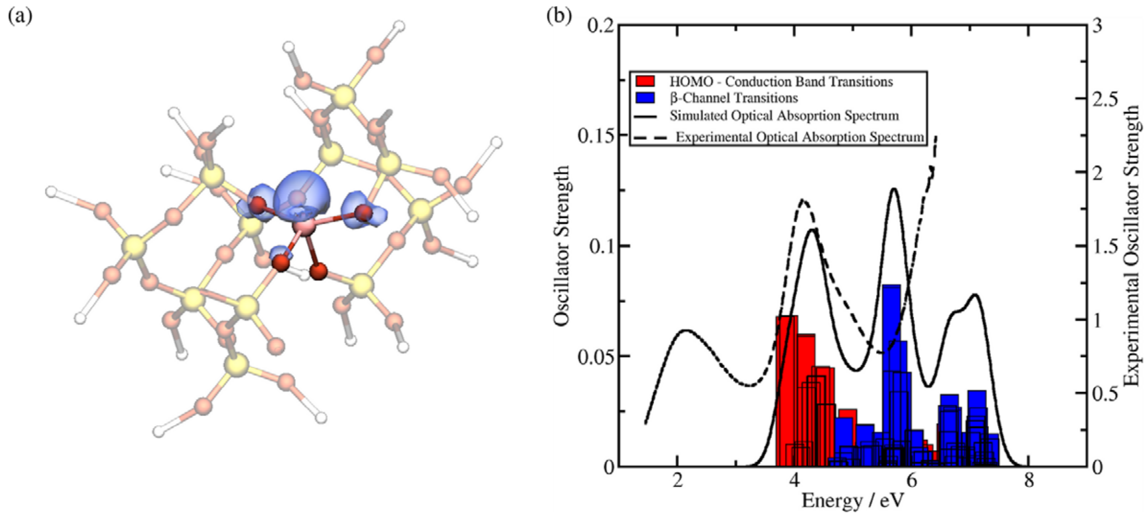

Figure 3. (a) Atomic structure and spin density of GEC in α quartz. The GeO_4 tetrahedron is highlighted, where the pink ball is Ge, the Si atoms are yellow balls, the O atoms are red balls and the spin density is the blue polyhedron. (b) Simulated and experimental optical absorption spectrum of the Ge electron trap in α quartz. The left y-axis is the calculated oscillator strength while the right y axis is the experimental oscillator strength. The dashed black line is an optical absorption spectrum of the Ge electron trap measured at 6 K. The solid black line is a sum of all Gaussian broadened excitation energies weighted by their respective oscillation strengths. The bar plot shows the excitation energies and their respective oscillation strengths. Red bars correspond to electronic transitions in the α channel while blue bars correspond to β channel.

the well-known Ge electron centre (GEC) in α-quartz, which has a similar structure to the electron trap considered here [16]. It is responsible for the Ge(I) EPR signal [29]. This signal strongly correlates with an optical absorption band at 4.2 eV, which is now universally attributed to this centre [17, 30–32]. Optical absorption spectra of Ge-doped SiO_2 include additional bands that peak at $\approx$5.8 eV and higher energies, which have also been tentatively assigned to GEC [33].

The quantum cluster containing 72 atoms and representing the α-quartz structure was embedded in the rest of the crystal as described above. A single Si atom at the centre of the quantum cluster was substituted for a Ge atom and the geometry of the system was optimized in the neutral charge state. The relaxation resulted in an extension of the Ge–O bonds to 1.72 Å compared to the Si–O bonds (1.64 Å) in α-quartz; however, the GeO_4 tetrahedron remains intact. The calculated band gap of the system is 7.2 eV with a Ge unoccupied state located just below the conduction band and strongly localized on the Ge atom.

An extra electron was then added to the system followed by full geometry optimization. This resulted in a strong local relaxation, where the O–Ge–O angle opened from 109° up to 148° and the extra electron highly localized on the Ge atom, as shown in figure 3(a). The Ge–O bond lengths extend asymmetrically, so that two bonds measure 1.83 Å while the other two bonds measure 1.87 Å. This defect introduces an occupied electron state which sits 5.0 eV below the α quartz conduction band.

The optical transition energies and oscillator strengths of the Ge electron trap in α quartz were then calculated using TDDFT. The obtained optical absorption spectrum is plotted as a solid black line in figure 3(b) along with the experimental spectrum which is plotted as a dashed black line. The experimental spectrum was obtained by by 1 MeV electron irradiation of Ge-doped α-quartz at 6 K followed by a measurement, also performed at 6 K. The 4.2 eV band can clearly be seen and this is the band that has been attributed to the GEC, while there is another band at 2.2 eV for the GEC's hole counterpart which is not considered in the calculation. The bar plot shows all calculated one-electron transitions. Each absorption line is Gaussian broadened by 0.3 eV in order to simulate homogeneous broadening. The total spectrum shown by the black line is a sum of broadened excitation energies, weighted by their respective oscillator strengths. The optical transitions can be categorised into two types. The transitions of the first type are highlighted as red bars while those of the second type are highlighted as blue bars. The first type is caused by transitions of the unpaired electron localized on the wide O–Ge–O angle into quasi-local states at the bottom of the a-SiO_2 conduction band (see also transition 1 in the inset of figure 4(b)). It exhibits a peak with a maximum at 4.2 eV, in excellent agreement with experiment. The second type is due to transitions of a β-spin electron from the occupied non-bonding oxygen 'p' orbitals, which have broken away from the top of the a-SiO_2 valence band due to the structural distortion introduced by the defect, to the unoccupied state which is localized on the wide O–Ge–O angle (see also transition 2 in the inset of figure 4(b)). They comprise 2 peaks with maxima at around 5.8 eV and 7.1 eV. The O 'p' states, which split from the top of the valence band, are localized around the wide O–Ge–O angle, similar to the O 'p' states of the nearest O neighbours highlighted in figure 3(a). The 5.8 eV peak agrees very well with the band recently assigned to the GEC in a-SiO_2 [33].

3.2. Optical absorption of the electron trapping centre

As has been shown in previous calculations [16], extra electrons can trap at certain (precursor) sites in amorphous SiO_2 networks without a barrier. These sites are characterized by

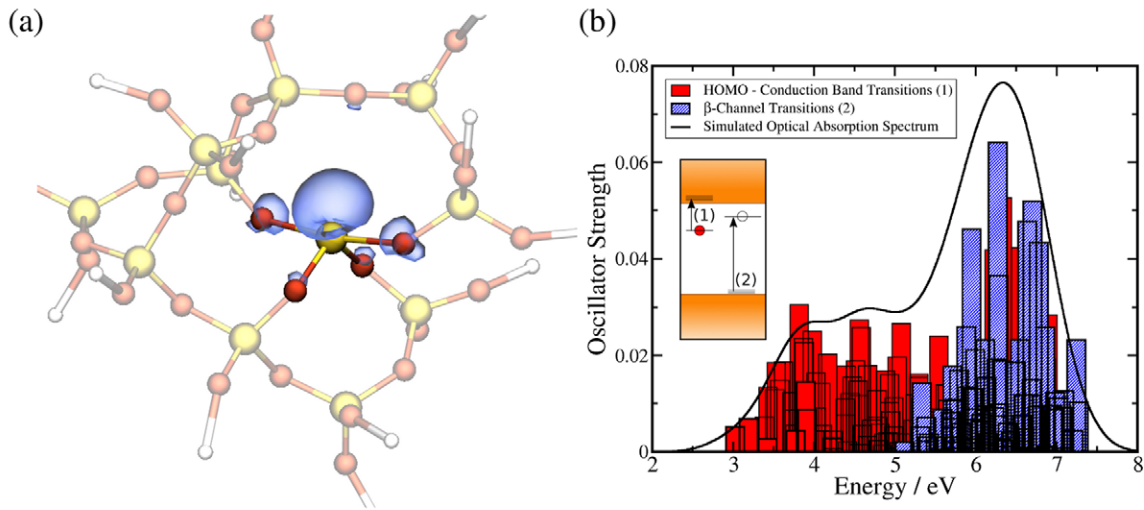

Figure 4. (a) The spin density of the electron localized in a-SiO_2. The tetrahedron with the wide O–Si–O angle is highlighted. Note that the colour scheme is the same as that of figure 3(a). (b) The calculated optical absorption spectrum of intrinsic electron traps in a-SiO_2. The inset shows a schematic of the optical transitions that can occur in the intrinsic electron trap. Two types of transitions are shown by two colours. See text for discussion.

strained Si–O bonds and O–Si–O angles greater than 132°. Although these angles are at the extreme of the distribution of O–Si–O angles in a-SiO_2, which peaks at ≈109.5°, we have estimated that the concentration of such precursor sites in our glass models is $\approx 4 \times 10^{19}$ cm^{-3} [16]. The electron trapping at network sites with O–Si–O angle less than 132°, requires overcoming an energy barrier and hence is less probable. After finding these sites in seven different a-SiO_2 models, a quantum region in an embedded cluster calculation was centred at a wide O–Si–O angle and included between 96 and 114 atoms. Due to the disorder in a-SiO_2 and the rather stringent criterion of O–Si–O angles greater than 132°, it was not possible to standardize the numbers of atoms described quantum mechanically across the seven different glass models. The quantum region was then interfaced with a classically polarizable region which contained between 910 and 933 atoms. The diameter of the entire system is ≈50 nm while the quantum regions are ≈1.5 nm in diameter. The positions of all atoms in region I were optimized in the neutral charge state. We also checked that the size of the region I is sufficient to accommodate the distortion induced by the electron localization in the amorphous network. The one-electron band gap averaged over the seven different samples in the embedded cluster model is 7.7 eV, ranging from 7.4 eV to 8.1 eV.

An extra electron was added into each of the seven samples and their respective geometries optimized, resulting in seven different intrinsic electron trap configurations, where an electron has localized at a precursor Si site and the O–Si–O angle has opened from 132° to an average of 174°, ranging over 5°. These electron traps introduce an occupied one-electron state located on average 4.3 eV below the bottom of the conduction band in the a-SiO_2 matrices, ranging between 3.7 and 4.8 eV. The spin density of this system is shown in figure 4(a).

The transition energies and oscillator strengths of all seven electron trapping configurations calculated using TDDFT are plotted together with equal weights in figure 4(b). The bar plot shows all optical transitions corresponding to the two types explained in the inset of figure 4(b) with their respective oscillation strengths. Each absorption line is Gaussian broadened by 0.3 eV to simulate homogeneous broadening and the black line in figure 4(b) is produced as a sum of all Gaussian broadened optical transitions in seven electron trapping centres weighted by their respective oscillation strengths. Transitions of the first type are highlighted as red bars while the second type are highlighted as striped blue bars. The first type is caused by the electron localized on the wide O–Si–O angle (see figure 4(a)) being excited into quasi-local states at the bottom of the a-SiO_2 conduction band composed of 'd' orbitals of nearby Si atoms and nearby O 's' orbitals. These transitions cause peaks with maxima at 3.7 and 4.7 eV. The second type is due to the excitation of a β-spin electron from the occupied non-bonding oxygen 'p' orbitals, which have broken away from the top of the a-SiO_2 valence band due to the structural distortion introduced by the intrinsic electron trap, into the unoccupied states in the band gap localized on the wide O–Si–O angle. They comprise a peak with a maximum at around 6.4 eV. These non-bonding O 'p' states are localized around the wide O–Si–O angle, similar to the O 'p' states of the nearest O neighbours highlighted in figure 4(a). The whole spectrum is much broader than that of the GEC in figure 3(b) because the transitions in each local defect configurations have different energies due to the disorder of a-SiO_2.

We note that the calculated spectrum exhibits transitions in the energy range of 3–7 eV. This is consistent with both the anneal and spectral bleaching data, which show a significant reduction of the optical density at energies exceeding 4 eV (see figure 1). The nature of both types of transitions is the same as in the GEC. The results of the thermal anneal at 186 K shown in figure 1(a) demonstrate that hole mobility causes complete bleaching of the optical absorption up to about 4.0 eV and partial depletion of bands at higher energies. This is consistent with our suggestion that the 3.7 eV band originates from the trapped electron centre created as a counterpart to self-trapped holes and indicates that the higher energy

bands are composites of optical absorption bands of trapped electrons as well as other defects. The first type of electron excitation would create electrons at the bottom of the a-SiO_2 conduction band, which would then recombine with holes and react with other defects. This explains why the optical excitation with 3.87 eV photons results in the bleaching of the 2.2 eV band and some of the E′ centres.

4. Conclusions

Our results provide the strongest evidence yet for the formation of intrinsic localized electron centres in a-SiO_2 as a counterpart to self-trapped holes and support a detailed theoretical model of a strongly localized electron in a disordered oxide. This localization is promoted by strained Si–O bonds and results in distorted SiO_4 tetrahedra. Therefore, one can expect that similar electron traps can exist in other types of silica glasses [34], feldspar and tectosilicates based on networks of SiO_4 tetrahedra. Many of these materials contain, as yet unexplained, deep electron centres responsible for thermo-luminescence employed in e.g. luminescence dating [1]. Therefore, we believe the optical signatures of intrinsic electron traps revealed here will be useful for understanding the properties and stability of other silicates, and electronic and optical devices utilizing a-SiO_2.

Acknowledgments

The authors acknowledge EPSRC and the EU FP7 project MORDRED (EU Project grant No. 261868) and COST Action CM1104 for financial support and the UK's HPC Materials Chemistry Consortium, which is funded by EPSRC (EP/F067496), for providing computer resources on the UK's national high-performance computing service HECToR and Archer. We are grateful to the London Centre for Nanotechnology for additional computing resources. A-M El-Sayed is grateful to the UK Doctoral Training Centre in Energy Demand Reduction and the Built Environment, funded by the EPSRC (EP/H009612/1). We thank V V Afanas'ev, A Alessi, L Skuja and K Kajihara for valuable and stimulating discussions.

References

[1] Kars R H, Poolton N R J, Jain M, Ankjærgaard C, Dorenbos P and Wallinga J 2013 *Radiat. Meas.* **59** 103–13
[2] Schubert M, Preis E, Blakesley J C, Pingel P, Scherf U and Neher D 2013 *Phys. Rev.* B **87** 024203
[3] Ellis B, Subramanya Herle P, Rho Y H, Nazar L F, Dunlap R, Perry L K and Ryan D H 2007 *Faraday Discuss.* **134** 119–141
[4] Balog R, Cicman P, Field D, Feketeova L and Hoydalsvik K 2011 *J. Phys. Chem.* A **115** 6820–4
[5] Griscom D L 1989 *Phys. Rev.* B **40** 4224–7
[6] Griscom D L 2006 *J. Non-Cryst. Solids* **352** 2601
[7] Kimmel A V, Sushko P V and Shluger A L 2007 *J. Non-Cryst. Solids* **353** 599–604
[8] Sicolo S, Palma G, Di Valentin C and Pacchioni G 2007 *Phys. Rev.* B **76** 075121
[9] Vigouroux J P, Duraud J P, Le Moel A, Le Gressus C and Griscom D K 1985 *J. Appl. Phys.* **57** 5139–44
[10] Shkrob I A and Trifunac A D 1997 *J. Chem. Phys.* **107** 2374–85
[11] Shkrob I A, Tadjikov B M, Chemerisov S D and Trifunac A D 1999 *J. Chem. Phys.* **111** 5124–40
[12] Afanas'ev V V and Stesmans A 1997 *Appl. Phys. Lett.* **71** 3844–6
[13] Afanas'ev V V, Stesmans A, Bassler M, Pensl G and Schulz M J 2000 *Appl. Phys. Lett.* **76** 336–8
[14] Houssa M, Tuominen M, Naili M, Afanasev V, Stesmans A, Haukka S and Heyns M 2000 *J. Appl. Phys.* **87** 8615–20
[15] Farnesi Camellone M, Reiner J C, Sennhauser U and Schlapbach L 2007 *Phys. Rev.* B **76** 125205
[16] El-Sayed A M, Watkins M B, Afanas'ev V V and Shluger A L 2014 *Phys. Rev.* B **89** 125201
[17] Sasajima Y and Tanimura K 2003 *Phys. Rev.* B **68** 014204
[18] Skuja L 1998 *J. Non-Cryst. Solids* **239** 16–48
[19] Kimmel A V, Sushko P V, Shluger A L and Bersuker G 2009 *ECS Trans.* **19** 3–17
[20] Pacchioni G, Skuja L, Griscom D L (eds) 2000 *Defects in SiO_2 and Related Dielectrics: Science and Technology* (*Nato Science Series*) (Boston, MA: Kluwer) pp 73–118
[21] Sushko P V, Shluger A L and Catlow C R A 2000 *Surf. Sci.* **450** 153–170
[22] van Duin A C T, Strachan A, Stewman S, Zhang Q, Xu X and Goddard W 2003 *J. Phys. Chem.* A **107** 3803–11
[23] Sulimov V B, Sushko P V, Edwards A H, Shluger A L and Stoneham A M 2002 *Phys. Rev.* B **66** 024108
[24] Mysovsky A S, Sushko P V, Mukhopadhyay S, Edwards A H and Shluger A L 2004 *Phys. Rev.* B **69** 085202
[25] van Beest B W H, Kramer G J and van Santen R A 1990 *Phys. Rev. Lett.* **64** 1955–8
[26] Lee C, Yang W and Parr R G 1988 *Phys. Rev.* B **37** 785
[27] Lany S and Zunger A 2009 *Phys. Rev.* B **80** 085202
[28] Marques M and Gross E 2004 *Annu. Rev. Phys. Chem.* **55** 427–55
[29] Isoya J, Weil J A and Claridge R F C 1978 *J. Chem. Phys.* **69** 4876
[30] Hayes W and Jenkin T J L 1986 *J. Phys. C: Solid state phys.* **19** 6211–9
[31] Jenkin T J L, Koppitz J and Hayes W 1987 *J. Phys. C: Solid State Phys.* **20** L367–71
[32] Girard S, Kuhnhenn J, Gusarov A, Brichard B, Van Uffelen M, Ouerdane Y, Boukenter A and Marcandella C 2013 *IEEE Trans. Nucl. Sci.* **60** 2015–36
[33] Alessi A, Agnello S, Grandi S, Parlato A and Gelardi F M 2009 *Phys. Rev.* B **80** 014103
[34] Trukhin A N, Tolstoi M N, Glebov L B and Savelev V L 1980 *Phys. Status Solidi* **99** 155–62